Stop-band structure in complementary three-dimensional opal-based photonic crystals

1999 J. Phys.: Condens. Matter 11 3593

(http://iopscience.iop.org/0953-8984/11/17/317)

J. Phys.: Condens. Matter **11** (1999) 3593–3600. Printed in the UK PII: S0953-8984(99)99397-9

Stop-band structure in complementary three-dimensional opal-based photonic crystals

S G Romanov†‡, A V Fokin‡ and R M De La Rue†

† Optoelectronics Research Group, Department of Electronics and Electrical Engineering, University of Glasgow, Glasgow G12 8QQ, UK
‡ A F Ioffe Physical Technical Institute, St Petersburg, 194021, Russia

Received 17 November 1998, in final form 8 March 1999

Abstract. The stop-band width and angular dispersion have been traced by angle-resolved reflectance spectroscopy for two opposite configurations of opal-based photonic crystals where either the silica balls possess a higher refractive index than the voids or vice versa. It has been demonstrated that filling the empty voids of opal with a material of higher refractive index than silica results in widening of the stop-band and squeezing of its dispersion, thus improving the stop-band of the opal grating towards the omnidirectional photonic band-gap situation.

1. Introduction

The dispersion of the photonic band-gap (PBG) in photonic crystals is one of the most important parameters defining whether the photonic crystal possesses an omnidirectional (complete) PBG or not. A prototype for three-dimensional (3D) photonic crystals operating in the visible range is the colloidal suspension and its solid counterpart, opal [1]. Opal is a natural grating consisting of closely packed identical balls where the light is scattered at the interfaces between the SiO_2 balls and the air in the voids between the balls. The light scattered from such a package peaks at a definite wavelength, which satisfies the Bragg condition. The refractive index (RI) contrast between silica ($n_{\mathrm{ball}} \approx 1.4$) and air is not high enough to provide complete PBG formation and, therefore, opal is an example of an incomplete-band-gap photonic crystal. However, opal can be used as a 'host' for impregnation of its voids with 'guest' material, thus providing substantial changes in the RI contrast (RIC) [2].

Optical propagation in the spectral range of an incomplete PBG acquires an anisotropy, which depends on the symmetry of the photonic crystal. For opal-based and colloidal crystals, the anisotropy of the stop-band has been revealed by changing the angle of incidence of the light [2–6]. For water-filled and bare opals, the stop-band angular dispersion was found to satisfy closely the fcc symmetry of the opal lattice according to Bragg's law [3, 4]. It was found also that with an increase in the RIC, the effectiveness of the Bragg scattering increases progressively and the stop-band widens and red-shifts [7, 5, 8–10]. The angular dispersion of the stop-band is the important parameter, because it shows the extent of the overlap of the stop-bands for different directions in the photonic crystal. However, to date no attempt has been made to compare the angular dispersions of the original opal and inverted opal. In what follows we use the definition of refractive index contrast RIC $= n_{\mathrm{ball}}/n_{\mathrm{guest}} - 1$ to distinguish, according to the sign of the RIC [11], whether the balls or the filled voids possess the higher index. In the present paper we have demonstrated the behaviour of the stop-band in

0953-8984/99/173593+08$19.50

complementary incomplete photonic crystal opals having empty voids and opals having voids infilled with sulphur.

2. Materials and experimental techniques

Opal is the fcc-type packing of amorphous silica-made balls, the deviation of whose diameter is $\Delta D/D < 5\%$. Figure 1(a) shows clearly the three dimensionality and the fcc nature of the opal grating since both square and hexagonal packings of balls coexist in intersecting (100) and (111) planes at random cleaves of the opal. Opal with a ball diameter of $D = 236$ nm was used in this study. SEM inspection revealed that opal samples were oriented with the closest-packed (111) planes parallel to the surface of the platelet. Opal host material for sulphur treatment was cut from a single larger piece and the remaining untreated material was then used for comparison. Complete infilling of the opal voids with sulphur was approached through impregnation with molten sulphur using the surface tension forces of liquefied sulphur on silica. The micrograph in figure 1(b) demonstrates the simulation of this void grating obtained by replacing sulphur with indium in order to visualize the opal replica using scanning electron microscopy. In what follows we shall label the empty opal 'air-opal' and the completely impregnated opal 'S-opal'.

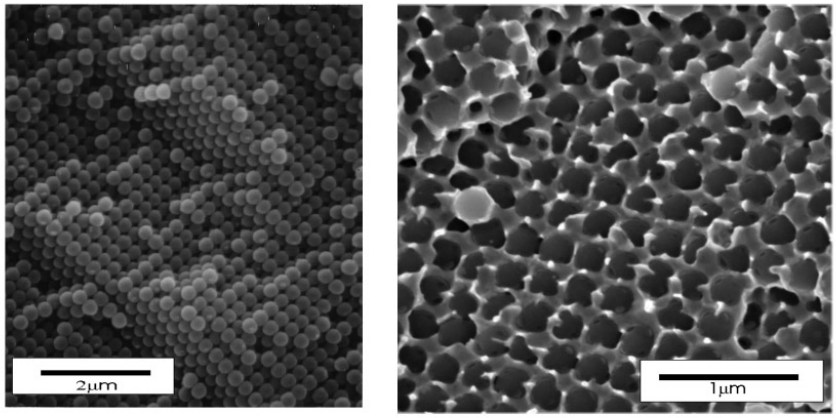

(a) (b)

Figure 1. SEM pictures of cleaved bare opal (a) and opal with impregnated voids (b).

There are two types of void in an fcc package of spherical balls: octahedral voids (O-voids) and tetragonal (T-voids), of which the diameters are $d_O = 0.41D$ and $d_T = 0.23D$, respectively [12]. This terminology does not describe the exact shape of the voids but describes that of the polyhedron which is formed by the silica balls surrounding the void. T-voids are formed between four and O-voids between six touching balls: the latter configuration is highlighted in figure 2. These voids are in turn arranged with fcc symmetry, but with the basis of a unit cell consisting of a total of one O-void and two T-voids, which is the basic difference between ball and void lattices. Figure 2 shows two adjacent (111) planes of an fcc ball package with O-voids situated between them, which is the configuration of scatterers actually used in our experiments. The spacing between the O-voids is the same as the ball spacing, but these lattices are offset when observed along a (111) axis.

Samples were cut in thin platelet sections with the (111) plane parallel to the large face of the platelet. This face was illuminated by monochromatic light selected from a Newport white-light source by a monochromator and the illuminated area was around 1 mm^2. The

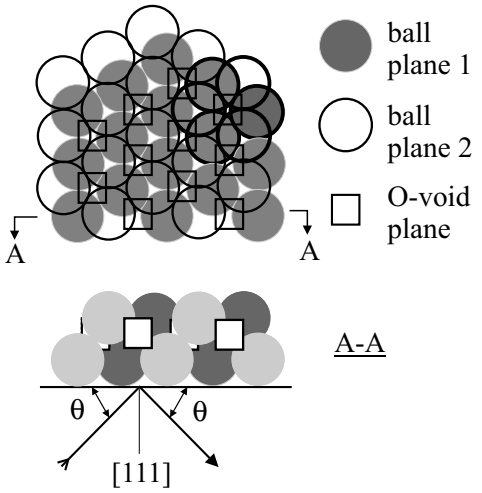

Figure 2. Schematic diagrams of ball and void arrangements along (upper panel) and across (lower panel) a stack of (111) planes. In the upper right-hand corner six balls (three from each plane), which surround the O-void, are highlighted by thicker borders. The scattering configuration used in the experiment is shown in the lower panel.

opal used was a textured polycrystal possessing monocrystalline facets of sub-millimetre-scale dimensions. The random disorientation of the (111) facets was up to 10°. We assume, therefore, that the spectra observed were averages over several slightly differently oriented areas. The transmission and reflectance spectra show a Bragg diffraction feature at the same wavelength if the light is incident normally on the sample surface. However, with off-normal optical incidence, the Bragg dip in the transmission rapidly disappears, while its counterpart in reflectance continues to be clearly resolved. Accordingly, reflectance spectroscopy was adopted for studies of the diffraction at oblique optical incidence. The depth sampled by reflectance depends self-consistently upon the scattering strength (see, e.g., the discussion in [13])—and therefore the reflectance data are free from the attenuation length effect [14]. Reflectance measurements were made on platelets approximately 0.5 mm thick by changing the angle of the incidence of the light beam with respect to the sample surface (angle θ) and collecting the forward-scattered light at the same angle (figure 2). Another rotation around the axis normal to the sample surface (angle φ) was made to examine the grating symmetry properties. Spectra were collected at angle-of-incidence steps of $\Delta\theta = 5^\circ$ in the range 90° to 45°, for light polarized both in-plane and perpendicular to the plane of incidence. Angular resolution around 2° was obtained by collimating the scattered beam.

Linear polarizers were used to select the $\boldsymbol{E}$-vector orientation of the incident and scattered light. It appears, however, that the scattered light does not preserve its polarization, as was clearly demonstrated by observations of the Bragg peak for cross-aligned polarizers. In what follows we show the reflectance spectra for the s wave (the optical $\boldsymbol{E}$-vector polarized perpendicular to the plane of incidence) by assuming that, in this case, the scattering is the same as for unpolarized light [15].

Opal is a non-ideal insulator because it has an absorption band in the range 1.7–3.5 eV caused by the oxygen vacancies in its silica skeleton [2, 16]. The extent of these defects depends on the details of the opal synthesis process and, therefore, effects related to the presence of the corresponding impurity-like band within the forbidden gap of silica appear differently when an alternative source of opals is used (see, e.g., [4]). Correspondingly, opal

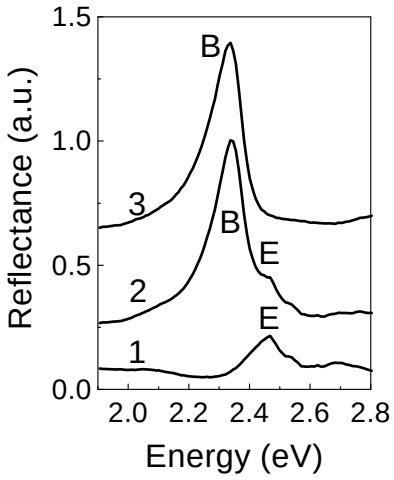

Figure 3. Reflectance spectra of disordered (curve 1) and ordered (curve 2) air-opals. Both the diffraction peak (B) and the peak from electronic absorption by the silica defects (E) are shown. Curve 3 is the diffraction peak (curve 2) after correction using the spectrum of disordered opal. The spectra are shifted along the vertical axis.

possesses uneven transmission and reflectance spectra irrespective of the degree of order in its porosity (figure 3). When scanning over the angle of incidence, θ, these features remain in the same spectral position—but change their magnitude. Furthermore, we use reflectance spectra of ordered opal, which are divided on those of disordered opal, in order to discriminate the stop-band-related variations only, first, and to take into account the scrambling of polarization, second.

3. Experimental results

Figure 4(a) shows the reflectance spectra of air-opal at directions ranging from nearly normal to the (111) crystalline planes ($\theta = 85^\circ$) round to $\theta = 45^\circ$. The peak in a spectrum corresponds to the interference maximum of the Bragg scattered light. The reflectance intensity at the peak exceeds the background scattering level by an order of magnitude, while the resolution of the peak is reduced at angles below 50°, being restricted by the increase of the background scattering due to the disorder of the opal package. Bragg resonance at $\theta = 90^\circ$ was also observed, but spectral decomposition is required to resolve it clearly. S-opal demonstrates a shift in the Bragg resonances to lower energy, widening of Bragg peaks and squeezing of their angular dispersion (figure 4(b)). In order to make a quantitative comparison of photonic crystals with different stop-band positions, the width of the Bragg peak ΔE at half-height was normalized with respect to the central energy of the peak, i.e. we have plotted $\Delta E/E_c$ (figure 5(a)).

From the set of reflectance spectra at different values of θ, the stop-band angular dependence $\Delta E(\theta)$ was extracted. Figure 6 compares the dispersion of $\Delta E(\theta)$ for air- and S-opals as the angle of incidence of the light changes from 90° to 45°. Remarkably, for S-opal the stop-band width increases but the stop-band angular dispersion *reduces* as compared with that of air-opal.

The effect of the rotation of the polarization plane upon the Bragg resonance was studied by rotation of the sample, which corresponds to tracing the stop-band position along an arbitrary

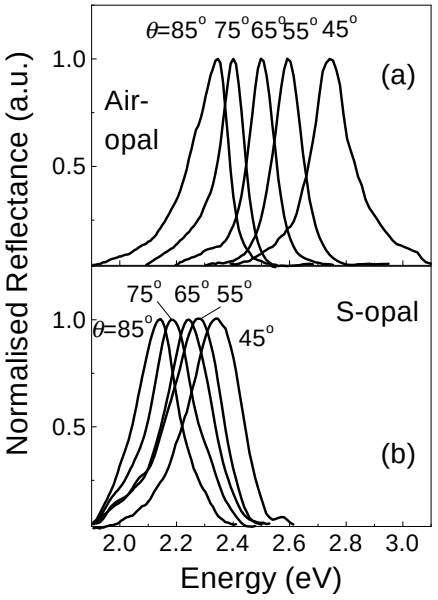

Figure 4. Bragg resonances at different angles of light incidence. (a) Air-opal; (b) S-opal. The numbers indicate the angle in degrees.

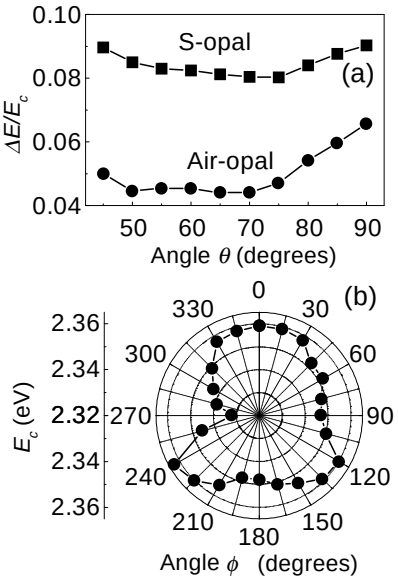

Figure 5. (a) The dependence of the relative stop-band width upon the angle of incidence for air-opal (circles) and S-opal (squares). (b) A polar graph of the azimuthal dependence of the stop-band centre of air-opal.

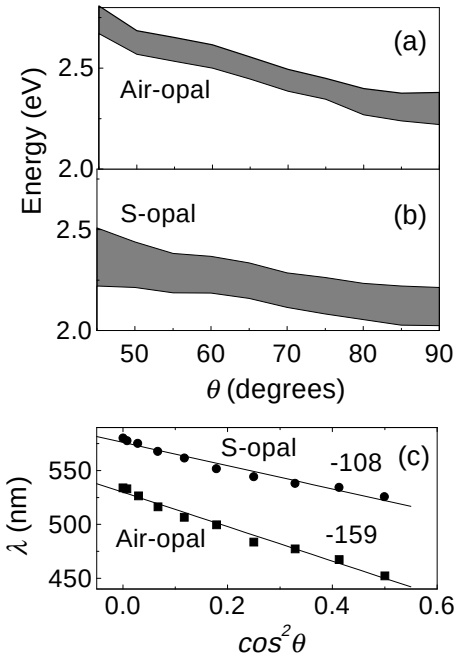

Figure 6. Angular dispersion of the stop-band FWHM in the range from $\theta = 90^\circ$ to 45° for air-opal (a) and S-opal (b). (c) The linearized dispersion of the stop-band in air- and S-opals. The numbers indicate the tangents.

circle around the L point of the Brillouin zone. A near 120°-periodic variation in the Bragg peak position is revealed (figure 5(b)), indicating the expected threefold symmetry for the (111) axis. This observation is in agreement with data from low-contrast opal composites [3].

4. Discussion

Ball lattices and O-void lattices have identical symmetry (see figure 2)—and therefore their reciprocal lattices are also identical. In consequence, the Bragg resonance of the scattered light occurs at the same point of the Brillouin zone for the two scattering ensembles. The basic difference between these crystals is the inversion of the scattering ensemble, since either the balls (air-opal) or the filled voids (S-opal) have a higher RI, giving positive, $n_{\mathrm{ball}}/n_{\mathrm{air}}-1=0.45$, and negative, $n_{\mathrm{ball}}/n_{\mathrm{S}}-1=-0.275$, RICs respectively, where $n_{\mathrm{ball}}=1.45$, $n_{\mathrm{S}}=2$.

Scatterers from all planes contribute to the crystal diffraction pattern simultaneously, with a weighting factor which is essentially a measure of the degree of filling of the planes with scatterers. The opal plane where the maximum scattering occurs is the most densely packed, (111), plane of an fcc lattice. Experiments [4, 6] and simulation [17] are in agreement in indicating that the contributions to the reflectance spectrum from planes other than (111) planes are less pronounced. This means that, practically, experiments on the Bragg scattering from a 3D opal-based grating at various angles of optical incidence primarily trace the position of the resonant scattering by the (111) planes.

A red-shift occurs in the Bragg peak after complete impregnation of opal with sulphur, due to the increase in the average RI of the grating n_{av} (figure 4). For a multiple-component composite, the average RI may be estimated as $n_{av}=\sum_i f_i n_i$, using the volume fraction f_i of the space occupied in the opal package by the component with RI n_i. This simplified expression has been found to correlate reasonably well with the Maxwell-Garnett approach [17]. Then, for opal with $f_{\mathrm{ball}}\approx 0.87$, the average indices are $n_{\mathrm{air-opal}}=1.39$ for air-opal and $n_{\mathrm{S-opal}}\approx 1.52$ for S-opal. The Bragg equation predicts a shift of the scattering peak according $\lambda_{\mathrm{S-opal}}/n_{\mathrm{air-opal}}\lambda_{\mathrm{air-opal}}=n_{\mathrm{S-opal}}/n_{\mathrm{air-opal}}$. Remarkably, the effective-medium estimate $n_{\mathrm{S-opal}}/n_{\mathrm{air-opal}}=1.09$ fits precisely the actual shift of the diffraction $\lambda_{\mathrm{S-opal}}/\lambda_{\mathrm{air-opal}}=582\ \mathrm{nm}/535\ \mathrm{nm}$.

The ratio of the output to the input in the Fourier domain is the transfer function of the system. While keeping the same lattice parameter, the inversion from air-opal to S-opal can be described as a spatial redistribution of the high-RI component. The Fourier transform of the variable part of the RI in a periodic ensemble of scatterers can be factorized into the structural factor, which describes the symmetry and ordering of the lattice, and the form factor, which describes the individual properties of the scatterers. Obviously the structural factor remains the same for air- and S-opal lattices with the same symmetry, but the form factor is certainly different and, as a result, the amplitude of the Fourier transform is also different. The observation of PBG enhancement in inverted opal is in agreement with theoretical analysis of the effects of complexity in the unit cell of a scattering lattice upon the PBG behaviour [18].

The scattering from the densely packed ensembles is essentially a collective effect and the scattering strength depends on both the size and the spacing of scatterers. The scattering cross-section of a dielectric sphere becomes several times greater than its geometrical cross-section when the Mie resonance frequency is approached, i.e. the resonance wavelength is $\lambda_{\mathrm{M}}\sim 2\pi D$, where D is the diameter of the sphere for which the RI is twice that of the background [19]. On the other hand, in the case of a periodic ensemble the scattered waves interfere to produce a diffraction pattern which satisfies the Bragg conditions. For a given RIC, the gap width $\Delta E/E_c$ approaches a maximum when the frequencies of the microscopic Mie and the coherent Bragg resonances are close to each other [15]. The filling factor of the high-RI component is the relevant parameter for the appearance of PBG-type behaviour because, for a periodic ensemble, it describes the correlation between the size and the spacing of the scatterers. To give an idea of the interplay between the size and the spacing of scatterers, we refer to the 1D case, where the optimal filling factor was estimated from the synergy of the two resonances as $f=1/(2n)$,

where n is the RI relative to the background [15]. From this point of view the optimal value $f_{\text{ball}} \approx 0.36$ should occur for air-opal, which is very far from the actual factor $f_{\text{ball}} \approx 0.87$. The same opal immersed in sulphur has a lower RI ratio, but the filling factor $f_{\text{S}} = 0.13$ of the S-opal is much closer to the estimated maximum of $f_{\text{S}} \approx 0.28$. It appears that, for this reason, the Bragg peak appears broader ($\Delta E/E_c$ increases) for S-opal than for air-opal. A full numerical simulation of the band structure using the plane-wave expansion method, like that applied to study several opal-related structures [20], is required to extract the more realistic dependence of the PBG width upon the filling factor for a given crystal.

In general, an incident wave can couple only with those eigenmodes of the photonic crystal which possess the same wavevector $\boldsymbol{k}$. In this situation, changes in the stop-band position ($E_c(\theta)$) with the angle of incidence are equivalent to probing different directions in the fcc Brillouin zone $E_c(k)$. In experimental studies of opals, changing the angle of incidence away from the (111) axis shows the variation of the stop-band starting from the L point of the Brillouin zone of an fcc crystal and then the occurrence of mixing on the way towards the high-symmetry points W, U and K at the edge of the Brillouin zone. The reason for the above uncertainty may be small misorientations of the (111) facets, which contribute differently to the scattering intensity. The correlation between the $\boldsymbol{k}$-vector and the angle for oblique incidence near the band-gap was addressed in reference [17], where the refraction at the sample boundaries has been taken into account. However, the effective RIs of air- and S-opals are very similar (1.39 versus 1.52), so we can neglect this difference as a first approximation and compare their stop-band dispersions directly. It has been shown that the angular dispersion of the Bragg peak appears linearized when it is plotted in λ–$\cos^2\theta$ coordinates if the Bragg law in the form $\lambda = 2d\sqrt{n_{av}^2 - \cos^2\theta}$ applies [4, 13]. The clear distinction between the stop-band dispersions of air- and S-opals is seen in figure 6(c). First, the increase of the effective RI of the crystal shifts the S-opal dispersion to longer wavelengths. Secondly, the redistribution of the high-RI component actually decreases the gradient of the S-opal dispersion. Both the red-shift and the squeezing of the stop-band dispersion are in line with band-structure calculations carried out for air-opal [21] and inverted opal respectively [20].

5. Conclusions

We have observed that inverting the lattice of scatterers in 3D photonic crystals based on opal hosts from a ball-related to a void-related ensemble of scatterers results in a dramatic change in the appearance of the stop-band. This inversion is associated with a broadening of the stop-band and squeezing of its angular dispersion. The main lesson from this work is a demonstration of the possibility of improving an incomplete photonic band-gap substantially via both an increase in the width of the stop-band and squeezing of the stop-band dispersion, while maintaining a situation of moderate refractive index contrast. When the scattering strength of the lattice increases, the squeezing of the (111) resonance dispersion increases progressively. The latter statement is definitively supported by observations of further squeezing of the stop-band angular dispersion for the case of CdS-opal [9] when compared with dispersion curves for air- and S-opals. This enhanced squeezing arises because CdS-opal possesses a higher RIC ($n_{\text{CdS}} \approx 2.7$) than that of S-opal. This observed behaviour supports the continuing hope of being able to design and produce 3D PBG materials with the technologically most common compound semiconductors as infill for the opal host. We emphasize that the angular dispersion of the stop-band is the relevant parameter for possible applications of PBG materials because it is this parameter that defines how photons incident from a range of different directions will interact with a photonic crystal.

Acknowledgments

This work was supported in part by the Leverhulme Trust (grant No F/179/AK) and the Russian Foundation for Basic Research (grant 96-02-17963).

References

[1] Sanders J V 1968 *Acta Crystallogr.* A **24** 427
[2] Romanov S G, Fokin A V, Butko V Y, Samoilovich S M and Sotomayor Torres C M 1996 *Phys. Solid State* **38** 1825
Romanov S G, Johnson N P, Fokin A V, Butko V Y, Yates H M, Pemble M E and Sotomayor Torres C M 1997 *Appl. Phys. Lett.* **70** 2091
[3] Bogomolov V N, Prokofiev A V and Samoilovich S M 1996 *Phys. Solid State* **38** 1493
[4] Lopez C, Miguez H, Vazquez L, Meseguer F, Mayoral R and Ocana M 1997 *Microstruct. Superlatt.* **22** 399
[5] Bogomolov V N, Gaponenko S V, Kapitonov A M, Prokofiev A V, Ponyavina A N, Silanovich N I and Samoilovich S M 1996 *Appl. Phys.* A **63** 613
[6] Tarhan I I and Watson G H 1996 *Phys. Rev. Lett.* **76** 315
[7] Bogomolov V N, Kurdukov D A, Prokofiev A V and Samoilovich S M 1996 *JETP Lett.* **63** 496
[8] Astratov V N, Vlasov Yu A, Karimov O Z, Kaplyanskii A A, Musikhin Yu G, Bert N A, Bogomolov V N and Prokofiev A V 1996 *Phys. Lett.* A **222** 349
[9] Romanov S G, Fokin A V, Alperovich V I, Johnson N P and De La Rue R M 1997 *Phys. Status Solidi* **164** 169
[10] Miguez H, Lopez C, Meseguer F, Blanco A, Vazquez L, Mayoral R, Ocana M, Fornes V and Mifsud A 1997 *Appl. Phys. Lett.* **71** 1148
[11] Vos W L, Sprik R, von Blaaderen A, Imhof A, Lagendijk A and Wegdam G H 1996 *Phys. Rev.* B **53** 16 231
[12] Balakirev V G, Bogomolov V N, Zhuravlev V V, Kumzerov Y A, Petranovsky V P, Romanov S G and Samoilovich L A 1993 *Crystallogr. Rep.* **38** 348
[13] Miguez H, Blanco A, Meseguer F and Lopez C 1999 *Phys. Rev.* B **59** 1563
[14] Vlasov Yu A, Astratov V N, Karimov O Z, Kaplyanskii A A, Bogomolov V N and Prokofiev A V 1997 *Phys. Rev.* B **55** R13 357
[15] John S 1995 *Photonic Band Gap Materials* ed C M Soukoulis (Dordrecht: Kluwer) p 563
[16] Dianov E M, Sokolov V O and Sulimov V M 1992 *J. Non-Cryst. Solids* **149** 5
[17] Yannopapas V, Stefanou N and Modinos A 1998 *J. Phys.: Condens. Matter* **9** 10 261
[18] Biswas R, Sigalas M M, Subramanian G and Ho K-M 1998 *Phys. Rev.* B **57** 3701
[19] van der Hulst H C 1981 *Light Scattering by Small Particles* (New York: Dover)
Jonker G N 1952 *Colloidal Science* ed H R Kruyt (Amsterdam: Elsevier) p 90
[20] Busch K and John S 1998 *Phys. Rev.* E **58** 3896
[21] Cassagne D 1998 *Ann. Phys., Paris* **24** 1